RESEARCH ARTICLE SUMMARY

PLANT SCIENCE

Glycosidase and glycan polymorphism control hydrolytic release of immunogenic flagellin peptides

Pierre Buscaill, Balakumaran Chandrasekar, Nattapong Sanguankiattichai, Jiorgos Kourelis, Farnusch Kaschani, Emma L. Thomas, Kyoko Morimoto, Markus Kaiser, Gail M. Preston, Yuki Ichinose, Renier A. L. van der Hoorn†

INTRODUCTION: Immunogenic flagellin fragments are a signature of bacterial invasion in both plants and animals. Plants recognize flagellin fragments via flagellin sensitive 2 (FLS2), a model receptor kinase that is highly conserved among angiosperms. However, little is known about events upstream of flagellin perception by FLS2. The flagellin fragments recognized by FLS2 are buried in the flagellin polymer structure and require hydrolytic release before recognition can occur, yet the hydrolases releasing these elicitors remain to be identified. Uncovering their identity is a daunting task because the extracellular space of plants (the apoplast) contains hundreds of uncharacterized glycosidases and proteases.

RATIONALE: We reasoned that pathogenic bacteria would suppress plant hydrolases that are important for immunity. To identify suppressed hydrolases in the apoplast of infected plants, we applied activity-based protein profiling with the use of chemical probes that irreversibly label the active site of hydrolases. We applied this strategy to study the infection of the tobacco relative *Nicotiana benthamiana* with the bacterial pathogens *Pseudomonas syringae* pv. *tabaci* (*Pta*6605), *P. syringae* pv. *syringae* (*Psy*B728a), and a virulent mutant of *P. syringae* pv. *tomato* [*Pto*DC3000(Δ*hQ*)].

RESULTS: Glycosidase activity profiling of apoplastic fluids isolated from *Pto*DC3000 (Δ*hQ*)-infected plants revealed that the activity of β-galactosidase 1 (BGAL1) is suppressed in the apoplast during infection. BGAL1 suppression is caused by a heat-stable, basic, small inhibitor molecule that is produced by the bacteria under the control of *hrpR/S/L* virulence regulators. Null mutants of *N. benthamiana* lacking BGAL1 generated by genome editing have substantially reduced apoplastic β-galactosidase activity and are more susceptible to *Pto*DC3000 (Δ*hQ*), demonstrating that BGAL1 contributes to immunity. When investigating how BGAL1 functions in immunity, we discovered that treatment of *Pto*DC3000(Δ*hQ*) and *Pta*6605 bacteria with apoplastic fluids containing BGAL1 results in the release of an elicitor that triggers a burst of reactive oxygen species in leaf discs, a signature immune response in plants. The released elicitor is flagellin derived because the triggered immune response requires both the FLS2 receptor in the plant and the flagellin-encoding *fliC* gene in the bacteria. More precisely, treatment of purified flagella with apoplastic fluids containing BGAL1 facilitates the release of immunogenic peptides from flagellin.

ON OUR WEBSITE

Read the full article at http://dx.doi.org/10.1126/science.aav0748

The flagellin polymer of both *Pto*DC3000 (Δ*hQ*) and *Pta*6605 is O-glycosylated with glycans consisting of several rhamnose residues and a terminal modified viosamine (mVio). Mutant *Pta*6605 bacteria carrying nonglycosylated flagellin, or carrying rhamnosylated flagellin lacking mVio, trigger the plant immune response when treated with apoplastic fluids, irrespective of BGAL1 presence, thus demonstrating that BGAL1 requires mVio for its function in immunity. Addition of a protease inhibitor cocktail to apoplastic fluids blocks the release of the flagellin elicitor from nonglycosylated flagellin, implicating apoplastic proteases in elicitor release acting downstream of BGAL1. Consistent with a specific role of BGAL1 in elicitor release, *bgal1* null mutants of *N. benthamiana* show increased susceptibility only to bacterial strains carrying mVio. Treatment of *Psy*B728a with apoplastic fluids containing BGAL1 does not facilitate release of the flagellin elicitor because its flagellin carries a different glycan moiety lacking mVio, thus providing protection against recognition.

CONCLUSION: Glycosidase BGAL1 acts upstream of proteases in the apoplast of *N. benthamiana* to release immunogenic peptides from glycosylated flagellin, but only on glycosylated flagellin containing mVio. *P. syringae* strains use both BGAL1 inhibitors and glycan polymorphism to suppress BGAL1 function and escape recognition. Glycan polymorphism is common to bacterial pathogens, indicating a general role for flagellin glycans in evading recognition of bacterial pathogens by both plants and animals. ■

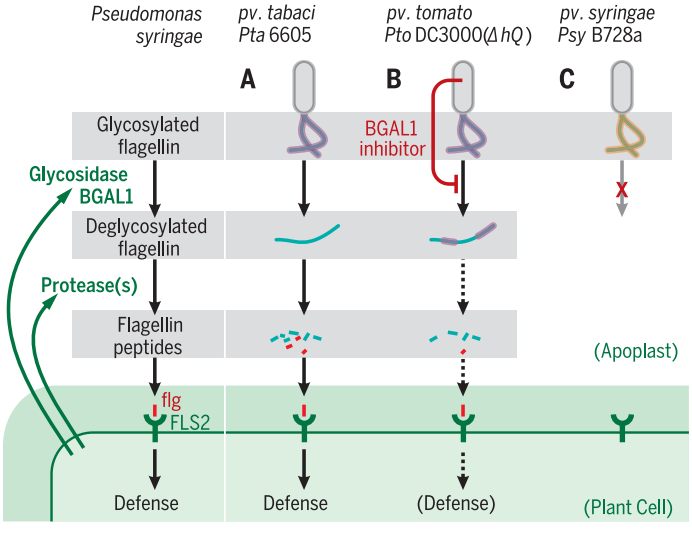

Control over hydrolytic release of immunogenic flagellin fragments. Secreted β-galactosidase BGAL1 and proteases contribute to immunity against bacteria with glycosylated flagellin carrying terminal mVio (purple) in both *Pta*6605 (**A**) and *Pto*DC3000(Δ*hQ*) (**B**) by releasing immunogenic peptides (flg, red) that are perceived by the FLS2 immune receptor. *Pto*DC3000(Δ*hQ*) (B) mitigates BGAL1 activity by the production of a BGAL1 inhibitor, whereas *Psy*B728a (**C**) produces BGAL1-insensitive glycans (orange) to escape recognition.

The list of author affiliations is available in the full article online.
†Corresponding author. Email: renier.vanderhoorn@plants.ox.ac.uk
Cite this article as P. Buscaill *et al.*, *Science* **364**, eaav0748 (2019). DOI: 10.1126/science.aav0748

RESEARCH ARTICLE

PLANT SCIENCE

Glycosidase and glycan polymorphism control hydrolytic release of immunogenic flagellin peptides

Pierre Buscaill[1], Balakumaran Chandrasekar[1]*, Nattapong Sanguankiattichai[1], Jiorgos Kourelis[1], Farnusch Kaschani[2], Emma L. Thomas[1], Kyoko Morimoto[1], Markus Kaiser[2], Gail M. Preston[1], Yuki Ichinose[3], Renier A. L. van der Hoorn[1]†

Plants and animals recognize conserved flagellin fragments as a signature of bacterial invasion. These immunogenic elicitor peptides are embedded in the flagellin polymer and require hydrolytic release before they can activate cell surface receptors. Although much of flagellin signaling is understood, little is known about the release of immunogenic fragments. We discovered that plant-secreted β-galactosidase 1 (BGAL1) of *Nicotiana benthamiana* promotes hydrolytic elicitor release and acts in immunity against pathogenic *Pseudomonas syringae* strains only when they carry a terminal modified viosamine (mVio) in the flagellin *O*-glycan. In counter defense, *P. syringae* pathovars evade host immunity by using BGAL1-resistant *O*-glycans or by producing a BGAL1 inhibitor. Polymorphic glycans on flagella are common to plant and animal pathogenic bacteria and represent an important determinant of host immunity to bacterial pathogens.

Plant pathogenic bacteria colonize the extracellular space within plant tissues (the apoplast) and manipulate their hosts with toxins and effector proteins delivered through the type III secretion system (T3SS) (*1*). Whereas these manipulation events inside the host cell are well studied, less is known about how bacteria manipulate the host apoplast.

One crucial aspect of plant–bacteria interactions is the recognition of extracellular pathogen-associated microbial patterns (PAMPs) that the plant can perceive, through pattern recognition receptors (PRRs), to mount PAMP-triggered immunity (PTI) (*2*). Most plants are able to recognize immunogenic peptides of bacterial flagellin through homologs of FLS2 (flagellin sensitive 2), a receptor kinase PRR (*2*, *3*). The 22–amino acid flagellin fragment flg22 has been intensively used to study receptor-like kinase (RLK) signaling and PTI in plants. Many T3SS-secreted effectors interfere in FLS2 signaling, underlining the important role of FLS2 signaling in immunity (*3*, *4*). However, although the release of immunogenic peptides like flg22 from the flagellin precursor protein has been anticipated, the mechanism by which this process occurs is unknown because these peptides are buried in the flagellin polymer structure (*5*). Identification of elicitor-releasing hydrolases is a daunting task because the plant apoplast contains hundreds of glycosidases, proteases, and other hydrolases (*6*, *7*).

We set out to discover the apoplastic hydrolases involved in immunity under the assumption that harmful host-secreted hydrolases will be suppressed by bacterial pathogens. To study apoplast manipulation, we investigated the interaction between *Nicotiana benthamiana* and the model bacterial pathogen *Pseudomonas syringae* pv. *tomato* DC3000 (*Pto*DC3000) (*8*). Whereas *Pto*DC3000 triggers nonhost resistance via recognition of the hopQ1-1 effector, the mutant lacking this type III effector [*Pto*DC3000 (Δ*hQ*)] is virulent on *N. benthamiana* (*8*).

Results

BGAL1 is inhibited during infection

To monitor the suppression of extracellular glycosidases, we applied glycosidase activity profiling on apoplastic fluids (AFs) isolated from infected plants and mock-inoculated control plants. Using the fluorescent activity–based probe JJB70, which labels the active site of glycosidases (*9*, *10*), we discovered a ~19-fold suppression of JJB70 labeling of a 45-kDa protein, previously identified as a putative β-galactosidase [BGAL1, NbS00024332g0007 (*10*)] (Fig. 1A). BGAL1 carries a signal peptide and is enriched in the apoplast (fig. S1). BGAL1 also accumulates in the apoplast when transiently overexpressed by infiltration of *N. benthamiana* with *Agrobacterium tumefaciens* (agroinfiltration) (Fig. 1B).

BGAL1 is a functional β-galactosidase because it can cleave galactose from FDG (fluorescein di-β-D-galactopyranoside) (fig. S2), and both JJB70 labeling and FDG hydrolysis by BGAL1 are blocked by the β-galactosidase inhibitor galactostatin (GSTN) (Fig. 1B). BGAL1 also selectively catalyzes hydrolyses of 4-nitrophenyl-β-galactopyranoside but not other monosaccharide conjugates (fig. S3). In contrast to active BGAL1, mutant BGAL1 protein carrying mutated catalytic residues [BGAL1^{E183A,E254A} (where E183A denotes Glu^{183}→Ala and E254A denotes Glu^{254}→Ala)] does not accumulate upon agroinfiltration (Fig. 1B). This nonaccumulating mutant BGAL1 is used as a "minus BGAL" (−BGAL1) control in follow-up experiments. Consistent with the strong suppression of JJB70 labeling in infected plants, FDG-hydrolyzing activity is reduced by a factor of ~30 in AFs upon infection (Fig. 1C).

Quantitative proteomic analysis indicated no change in the amounts of BGAL1 protein in AFs of infected plants (fig. S4), suggesting that BGAL1 is inactivated during infection. To test whether AFs of infected plants contain a BGAL1 inhibitor, we mixed AFs from infected and noninfected plants before and after JJB70 labeling, a method we term "convolution ABPP" [activity-based protein profiling (*11*)]. AFs from infected plants could suppress both JJB70 labeling (Fig. 1A) and FDG-hydrolyzing activity (Fig. 1C) present in AFs from the mock control, indicating that AFs from infected plants contain a BGAL1 inhibitor (Fig. 1D). The BGAL1 inhibitor is detected early during infection (fig. S6A) and also when *Pto*DC3000(Δ*hQ*) is grown in T3SS-inducing minimal media (fig. S5B). Inhibitor production is absent in Δ*hrpR*, Δ*hrpS*, and Δ*hrpL* mutants but present in Δ*hrpA* and Δ*hrcC* mutants of *Pto*DC3000, demonstrating that BGAL1 inhibitor production is controlled by virulence regulators but does not require the T3SS system (fig. S5B). The BGAL1 inhibitor is a heat-stable molecule of <3 kDa (fig. S6A) that is hydrophilic and basic (fig. S6, B and C). This BGAL1 inhibitor does not suppress the activity profiles of other hydrolases (fig. S6D) but remains to be identified.

BGAL1 contributes to immunity

We next investigated why *Pto*DC3000 inhibits BGAL1. BGAL1 is one of the 28 putative glycosyl hydrolases of family 35 (GH35) of *N. benthamiana* (fig. S7). *N. benthamiana* is an ancient alloploid, and BGAL1 has one putative homeolog, which has been pseudogenized (fig. S8A). Using genome editing with CRISPR-Cas9 (*12*), we generated two independent *BGAL1* null mutants: *bgal1-1* and *bgal1-2* (Fig. 2A and fig. S8). Both *bgal1* mutants contain frameshift mutations in the *BGAL1* open reading frame (fig. S8B), and BGAL1 depletion causes no major growth or developmental phenotypes (Fig. 2B). AFs from both *bgal1* mutants lack the JJB70 signal corresponding to BGAL1 (Fig. 2C) and have strongly reduced FDG hydrolyzing activity (Fig. 2D). Upon spray inoculation with *Pto*DC3000(Δ*hQ*), both *bgal1* mutants support enhanced bacterial growth (Fig. 2E) and develop more disease symptoms (Fig. 2F), confirming a role for BGAL1 in immunity. A similar increase in susceptibility was observed upon depletion of *BGAL1* transcripts by virus-induced gene silencing (VIGS) (fig. S9).

[1]Department of Plant Sciences, University of Oxford, Oxford, UK. [2]ZMB Chemical Biology, Faculty of Biology, University of Duisburg-Essen, Essen, Germany. [3]The Graduate School of Environmental and Life Science, Okayama University, Japan. *Present address: Institut für Pflanzliche Zellbiologie und Biotechnologie Heinrich-Heine-Universität, Düsseldorf, Germany. †Corresponding author. Email: renier.vanderhoorn@plants.ox.ac.uk

BGAL1 facilitates release of flagellin elicitor

We hypothesized that BGAL1 contributes to immunity by releasing an elicitor from bacteria that triggers a burst of reactive oxygen species (ROS), a signature immune response in plants. We therefore established an elicitor-release assay based on the incubation of bacteria with AFs and detection of released elicitors in a ROS burst assay using leaf discs of unchallenged plants (Fig. 3A).

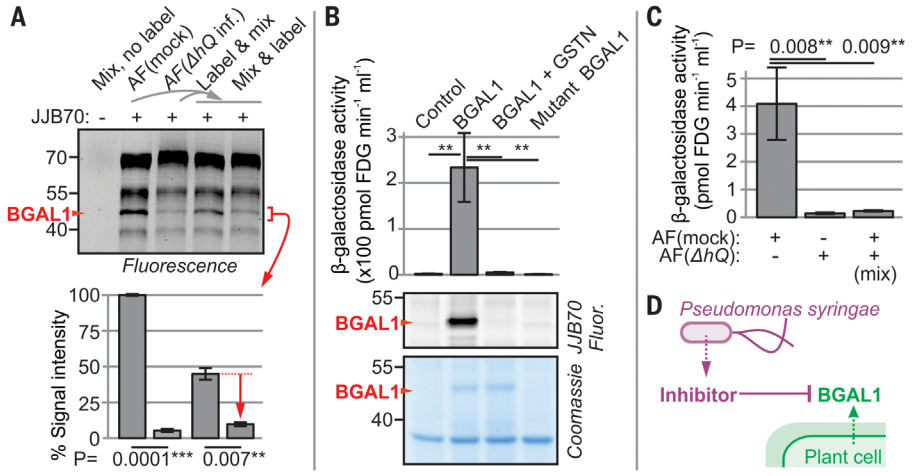

Fig. 1. BGAL1 is suppressed during bacterial infection. (**A**) BGAL1 labeling is suppressed in AFs of infected plants at 2 days postinfection (dpi). The two samples were also mixed in a 1:1 ratio before (mix and label) and after (label and mix) labeling with JJB70. The quantified fluorescence of the BGAL1 signal is plotted below. Error bars indicate mean ± SE of $n = 3$ replicates; t test was used to determine P values. (**B**) BGAL1 has β-galactosidase activity. FDG-hydrolyzing activity was measured on AFs isolated from leaves transiently expressing the silencing inhibitor P19 alone (control) or with BGAL1 (+) or mutant BGAL1 (−), pre-incubated with or without 10 μM galactostatin (GSTN). Error bars indicate mean ± SE of $n = 4$ replicates; Tukey HSD was used to determine P values. The samples were also labeled with JJB70 and stained with Coomassie. (**C**) Reduced β-galactosidase activity in AF from infected plants isolated at 2 dpi. The two samples were also mixed in a 1:1 ratio before FDG was added. Error bars indicate mean ± SE of $n = 5$ replicates; Tukey HSD was used to determine P values. (**D**) Schematic diagram showing BGAL1 and its inhibitor.

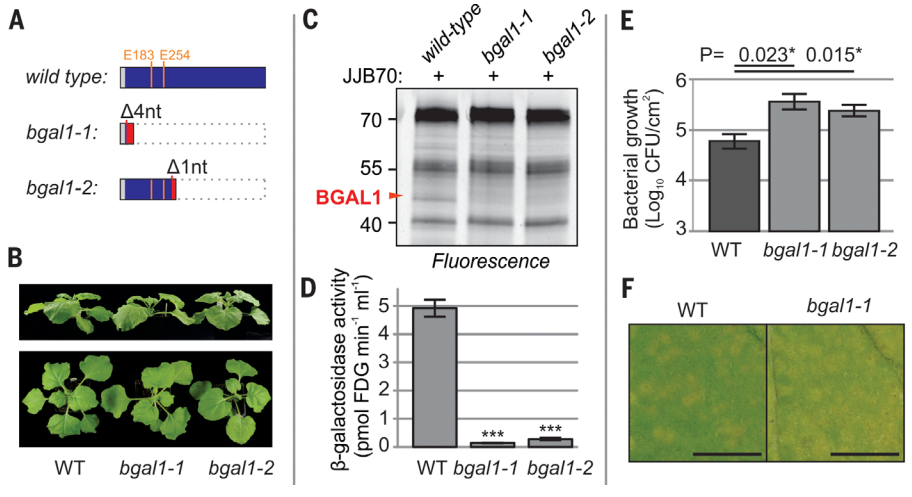

Fig. 2. BGAL1 contributes to immunity. (**A**) Open reading frames of wild type and two independent *bgal1* null mutants generated by genome editing (red, out-of-frame translation; orange, catalytic Glu residues). (**B**) Representative photos of 5-week-old plants. (**C**) Both *bgal1* null mutants lack the BGAL1 signal in the JJB70 labeling profile. (**D**) AF from both *bgal* mutants has reduced β-galactosidase activity. Error bars indicate mean ± SE of $n = 3$ replicates; Tukey HSD was used to determine ***P values < 0.001. (**E**) Compared with the wild type, both *bgal1* mutants are less resistant to *Pto*DC3000(Δ*hQ*). Bacterial growth of *Pto*DC3000(Δ*hQ*) upon spray inoculation was measured at 3 dpi. Error bars indicate mean ± SE of $n = 4$ replicates; t test was used to determine *P values. CFU, colony-forming units. (**F**) Representative photos of spray-infected leaves showing symptoms of bacterial spot disease at 6 dpi. Scale bars, 1 cm.

The ROS burst was induced in leaf discs of *N. benthamiana* when treated with bacteria that were incubated with AF from leaves overexpressing BGAL1 (Fig. 3B). The ROS burst was also absent when bacteria were omitted (fig. S10), indicating that the elicitor is derived from the bacteria. A similar BGAL1-dependent ROS burst was triggered in leaf discs of *Arabidopsis thaliana* (Fig. 3C), indicating that the BGAL1-released elicitor is recognized by different plant families.

We next found that *Arabidopsis* mutants lacking glycan receptors LORE or CERK1, or lacking both LYM1 and LYM3, still perceive the elicitor (fig. S11), indicating that the BGAL1-released elicitor is not related to lipopolysaccharide, chitin, or peptidoglycan, respectively (*13*–*15*). The ROS burst was also unaffected in leaf discs lacking SOBIR1 (fig. S11D) but was absent in leaf discs lacking BAK1 (Fig. 3D), indicating that elicitor perception involves a membrane-localized RLK but not a receptor-like protein (*3*). When testing BAK1-dependent immune RLKs, we discovered that leaf discs of the *Arabidopsis* mutant lacking FLS2, the RLK mediating flagellin recognition (*16*), are blind to the BGAL1-released elicitor (Fig. 3E). Likewise, *N. benthamiana* plants silenced for the *FLS2* ortholog [*NbFls2* (*17*)] were unable to sense the BGAL1-released elicitor (Fig. 3F). By contrast, an *Arabidopsis* mutant lacking EFR, the receptor for fragments of the bacterial EF-Tu protein, still perceives the BGAL1-released elicitor (fig. S11E).

Consistent with flagellin recognition via FLS2, BGAL1 treatment of mutant bacteria lacking flagellin [*Pto*DC3000(Δ*hQ*Δ*fliC* (*18*)] did not trigger the ROS burst in *Arabidopsis* (Fig. 3G) or *N. benthamiana* (Fig. 3H), indicating that the BGAL1-released elicitor is derived from flagellin. Indeed, treatment of purified flagellin with AFs containing BGAL1 also releases the elicitor (Fig. 3I), demonstrating that BGAL1 facilitates elicitor release directly from flagellin. Mass spectrometric analysis of peptides released from purified flagellin by AFs containing BGAL1 revealed several peptides known to trigger immunity (*19*) (fig. S12). These data demonstrate that BGAL1 controls the release of immunogenic peptides from flagellin.

BGAL1 acts on glycosylated flagellin

A conserved fragment of 22 amino acid residues of flagellin (flg22) containing the immunogenic sequence KINSAKDDAAGLQ (K, Lys; I, Ile; N, Asn; S, Ser; D, Asp; G, Gly; L, Leu; Q, Gln) [flg15-Δ2 (*19*)] is universally recognized in angiosperms by orthologs of FLS2 (*19*–*22*). This immunogenic region resides inside the flagellin rod (Fig. 4 and fig. S13) and has to be unfolded and excised before it can interact with FLS2 (*5*, *23*). The solvent-exposed surface of flagella is covered with *O*-glycans linked to six serine residues located in the D2 and D3 domains of each flagellin protein (Fig. 4). The *O*-glycans of *Pto*DC3000 consist of two or three rhamnose residues and a terminal modified viosamine (mVio) (*24*, *25*) (Fig. 4).

The involvement of BGAL1 in the release of the flagellin elicitor suggests that BGAL1 acts on

glycosylated flagellin and that glycan removal exposes the flagellin protein to proteases that release the flagellin elicitor (Fig. 5). We tested this hypothesis using *P. syringae*. pv. *tabaci* 6605 (*Pta*6605), which is also pathogenic on *N. benthamiana* (*26*) and has been used as a model to elucidate the glycan structure on the flagellin. The *O*-glycans on the flagellin of *Pta*6605 are identical to those of *Pto*DC3000 (Fig. 6A) (*24*, *25*, *27*), but *Pta*6605 does not produce a BGAL1 inhibitor (fig. S14). As with *Pto*DC3000(Δ*hQ*), BGAL1-treatment of *Pta*6605 bacteria releases an elicitor detected in both *N. benthamiana* (Fig. 6B) and *Arabidopsis* (fig. S15A), and *Pta*6605 grows better on *N. benthamiana bgal1* mutants than on wild-type (WT) plants (Fig. 6C). The elicitor released by BGAL1 is derived from flagellin, as it is undetected in *N. benthamiana* and *Arabidopsis* lacking *Nb*FLS2 and FLS2, respectively (fig. S15, B and C), and the elicitor is not released from *Pta*6605(Δ*fliC*) lacking flagellin (fig. S15D).

Next, we took advantage of *Pta*6605 mutants that lack different enzymes involved in the *O*-glycan formation on flagellin. Incubation of *Pta*6605(Δ*fgt1*) bacteria, which carries unglycosylated flagellin (Fig. 6D) (*27*), with AFs releases the elicitor, irrespective of BGAL1 presence (Fig. 6E). Accordingly, *Pta*6605(Δ*fgt1*) bacteria grew less when compared with *Pta*6605(WT), and BGAL1 no longer contributed to immunity because Δ*fgt1* bacteria grew equally well on both WT plants and *bgal1* mutant plants (Fig. 6F). *Pta*6605 mutants producing flagella that lack one *O*-glycosylation site [S143A, S164A, S176A, S183A, S193A, and S201A mutants, respectively (*27*)] also released the elicitor when incubated with AFs, even in the absence of BGAL1 (fig. S16). Consistent with the implicated role of proteases in the release of flagellin fragments, elicitor release from *Pta*6605(Δ*fgt1*) bacteria and purified non-glycosylated flagellin was blocked with a protease inhibitor cocktail (fig. S17). These data demonstrate that *O*-glycans on flagellin provide protection against hydrolytic elicitor release and that BGAL1 overcomes this protection.

BGAL1's role is specific for mVio glycans

To further specify BGAL1 action, we tested the *Pta*6605 mVio transferase mutant Δ*vioT* and mVio biosynthesis mutants Δ*vioA* and Δ*vioB*, which all carry flagellin with rhamnose *O*-glycans that lack the terminal mVio residue (Fig. 6G) (*28*). Like the Δ*fgt1* mutant, incubation of Δ*vioT*, Δ*vioA*, and Δ*vioB* mutant bacteria with AFs released the flagellin elicitor irrespective of BGAL1 presence (Fig. 6H and fig. S18), and these mutant bacteria grew equally well on WT and *bgal1* mutant plants (Fig. 6I and fig. S18). These data demonstrate that rhamnosyl glycans on flagella do not prevent elicitor release in the apoplast and indicate that mVio protects against elicitor release. These data also show that BGAL1-mediated elicitor release and the role of BGAL1 in immunity requires mVio on the flagellin glycans.

All *P. syringae* bacteria produce O-glycosylated flagella but the structures of the *O*-glycans can differ between strains. For instance, *P. syringae* pv. *syringae* B728a (*Psy*B728a), which has been isolated from bean but is also pathogenic on *N. benthamiana* (*29*), does not carry a (1,3)-linked

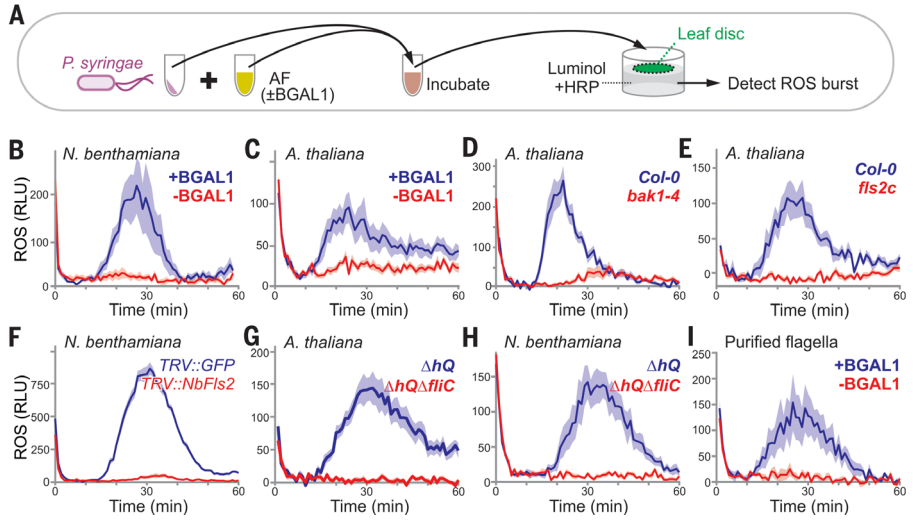

Fig. 3. BGAL1 controls the release of the flagellin elicitor. (**A**) Experimental procedure to detect BGAL1-released elicitors from bacteria. The pellet of a bacterial culture was resuspended and incubated with AF isolated from *N. benthamiana* leaves transiently overexpressing BGAL1 (+) or the minus BGAL control (−). The treated bacteria were added to leaf discs floating on a solution containing luminol and horseradish peroxidase (HRP), and ROS was detected over time by chemiluminescence. The ROS burst is triggered in leaf discs of *N. benthamiana* (**B**) and *Arabidopsis* (**C**) after pretreatment of bacteria with AFs from plants overexpressing BGAL1 (+BGAL1) but not the nonaccumulating mutant BGAL1 (−BGAL1). This ROS burst requires BAK1 (**D**) and FLS2 (**E**) and its ortholog NbFLS2 in *N. benthamiana* (**F**). The ROS burst also requires the flagellin-encoding *fliC* gene in *Pto*DC3000 in both *Arabidopsis* (**G**) and *N. benthamiana* (**H**), and is also induced in *N. benthamiana* by purified flagella treated with AF containing BGAL1 (**I**). Error intervals (shaded regions) indicate mean ± SE of $n = 6$ [(B) and (I)] or $n = 12$ [(C) to (H)] replicates. RLU, relative luminescence units.

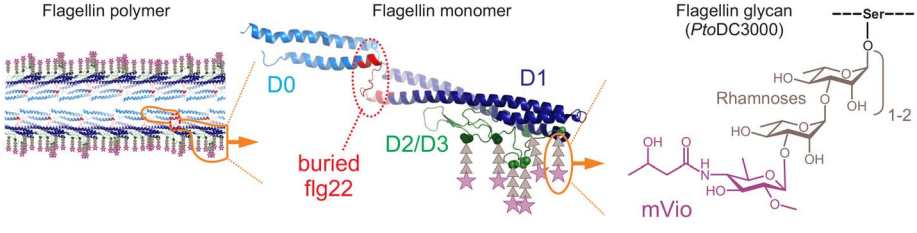

Fig. 4. Flagellin is a glycosylated protein polymer with a buried immunogenic sequence. Flagellin of *Pto*DC3000 was modeled on the basis of the flagellin polymer structure of *P. aeruginosa* (5wk5). Positions of O-glycosylated Ser residues (green) are distributed over the surface of the polymer.

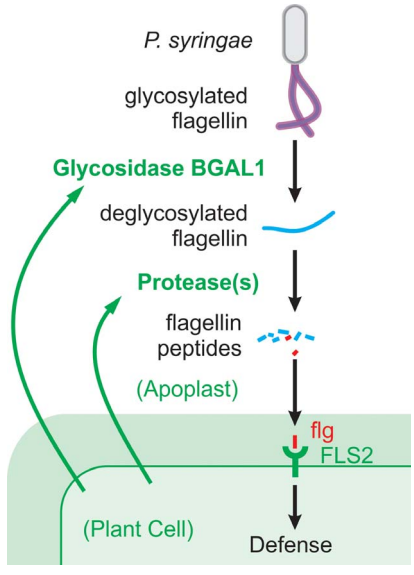

Fig. 5. Hydrolytic release of immunogenic peptides from flagellin. We hypothesize that BGAL1 controls the release of immunogenic flagellin elicitors (e.g., flg, red) from *P. syringae* by initiating the removal of the glycan protection layer from flagella. Proteases would then process flagellin to release the peptide elicitors, which are recognized by the FLS2 surface receptor.

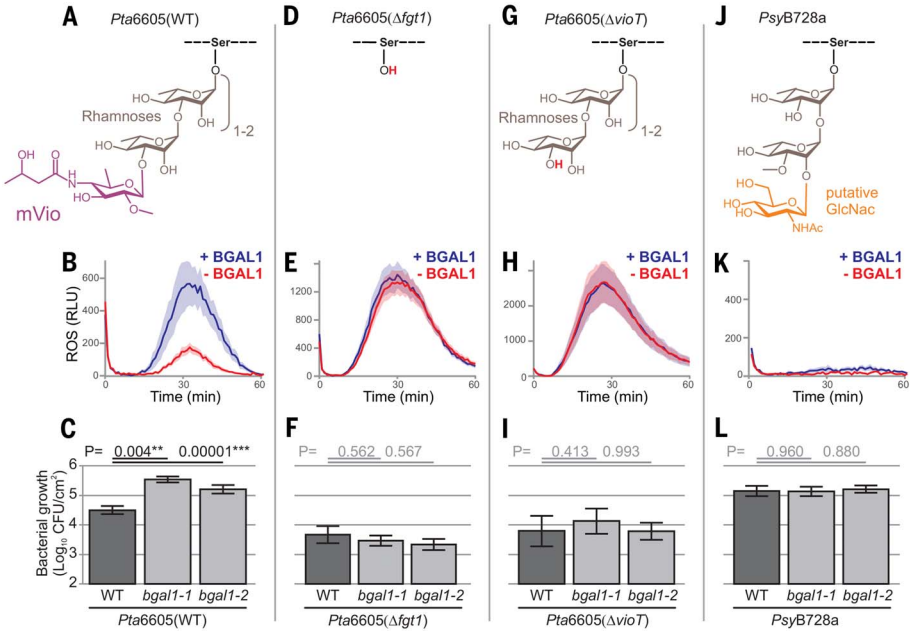

Fig. 6. BGAL1 acts in immunity only on bacteria carrying mVio on flagellin *O*-glycans. (**A** to **C**) BGAL1 also releases an elicitor from *Pta*6605. (**D** to **F**) BGAL1 is not required to release the flagellin elicitor from *Pta*6605(Δ*fgt1*) producing nonglycosylated flagellin. (**G** to **I**) BGAL1 is not required to release the flagellin elicitor from *Pta*6605(Δ*vioT*) lacking the terminal mVio. (**J** to **L**) BGAL1 does not release the flagellin elicitor from *Psy*B728a carrying a different flagellin glycan. (A, D, G, and J) Structures of flagellin *O*-glycans, determined previously. (B, E, H, and K) ROS burst assays of elicitor fractions from bacteria treated with AFs from plants overexpressing BGAL1 (+BGAL1) or mutant BGAL1 (-BGAL1). Error intervals (shaded regions) indicate mean ± SE of $n = 12$ replicates. (C, F, I, L) *Pta*6605 growth at 3 dpi on WT and *bgal1* mutant plants after spray inoculation. Error bars indicate mean ± SE of $n = 3$ (F), $n = 6$ (I), or $n = 8$ [(C) and (L)] replicates; *t* test was used to determine *P* values.

mVio but instead carries a putative (1,2)-linked terminal GlcNac [*N*-acetylglucosamine, Fig. 6J (*24*, *25*)]. Treatment of *Psy*B728a with AFs containing BGAL1 does not release the flagellin elicitor (Fig. 6K), and *Psy*B728a also grows equally well on WT and *bgal1* mutant plants (Fig. 6L). *Psy*B728a does not produce a BGAL1 inhibitor (fig. S14) and may suppress elicitor release through other mechanisms. These data indicate that the flagellin glycan of *Psy*B728a is protected against BGAL1 from *N. benthamiana*. However, plants silenced for NbFls2 are more susceptible to *Psy*B728a (*17*), which indicates that *N. benthamiana* has hydrolases that can release the flagellin elicitor from *Psy*B728a. We did not detect this activity in our elicitor-release assays, possibly because these hydrolases are not sufficiently present or active in the isolated AFs used. Overexpression of these hydrolases might overcome this limitation, as we discovered for BGAL1.

Discussion

Hydrolytic release of immunogenic peptides

We discovered that BGAL1 acts in immunity by controlling the release of immunogenic flagellin peptides and that bacteria counter the role of BGAL1 by producing a BGAL1 inhibitor or BGAL1-insensitive glycans. Our work also elucidates an important role for proteases in the release of immunogenic peptides. The *N. benthamiana* apoplast contains nearly 200 proteases that may act redundantly (*7*), and our strategy to identify hydrolases that are suppressed during infection may be useful for identifying the proteases that act in the release of the flagellin elicitor. We anticipate a similar important role for BGAL1 and other hydrolases in the release of different immunogenic flagellin fragments that are recognized in tomato and rice (*30*, *31*). Hydrolytic release of immunogenic peptides from precursors may also be required for peptide elicitors elf18, nlp24, and possibly pep13 from bacterial, fungal, and oomycete pathogens because these are also buried within folded protein structures (*32*–*36*). It will be interesting to determine whether the role of BGAL1 and proteases is conserved across plant species or whether host-specific hydrolytic processes dictate elicitor release and host specificity.

Glycan polymorphism as a common defense strategy

*Psy*B728a evades flagellin hydrolysis and recognition by the host, which suggests that polymorphic glycans on flagellin might help other plant-pathogenic bacteria evade recognition. Indeed, 2150-Da glycan moieties on flagellin in strain K1 of the bacterial rice pathogen *Acidovorax avenae* (*Ac*K1) prevent flagellin recognition in rice, whereas 1600-Da glycan moieties on flagellin from the related *Ac*N1141 strain do not prevent flagellin recognition (*37*). Likewise, despite being identical in protein sequence, the glycosylated flagellin of *P. syringae* pv. *glycinea* (*Psg*) triggers cell death in tobacco (*Nicotiana tabacum*) but the glycosylated flagellin of *Pta*6605 do not, probably owing to the distinctive *O*-glycan moieties (*38*, *39*). These observations indicate that polymorphic glycans are an important determinant in evading host immunity and that host plants secrete specialized glycosidases to release immunogenic flagellin fragments.

The role of flagellin glycans in host immunity evasion also extends to animal-pathogenic bacteria. Flagellin glycosylation mutants of *Pseudomonas aeruginosa*, for instance, are less virulent in wound infection assays in mice (*40*). Likewise, non-glycosylated flagellin proteins from the opportunistic human pathogen *Burkholderia cenocepacia* stimulate stronger TLR5-dependent immune responses in human cell lines when compared with glycosylated flagellin (*41*). Glycans on flagellin are also polymorphic in animal-pathogenic bacteria (*42*). For instance, *B. cenocepacia*, *Burkholderia pseudomallei*, and *Burkholderia thailandensis* carry different glycans that may provide different levels of protection against host hydrolases (*43*). These data indicate that polymorphic glycans on flagella are a common strategy to evade host immunity driven by host-specific hydrolases in both plants and animals.

Materials and methods

Plants

Nicotiana benthamiana plants were grown in a growth chamber at 21°C and ~60% relative humidity with a 12-hour photoperiod and a light intensity of 2000 cd·sr m^{-2}. *Arabidopsis* plants were grown in a Fitotron growth chamber (Weiss Gallenkamp, Loughborough, UK) at 21°C and ~60% relative humidity with a 12-hour photoperiod. *Arabidopsis* mutants used are all in *Col-0* background and are summarized in Table 1.

Bacterial strains

The *P. syringae* strains used in this study are listed in Table 2. *Pst*DC3000 strains were grown in Luria-Bertani (LB) medium with 50 μg/ml rifampicin at 28°C. *Pta*6605 strains were grown in King's B (KB) medium at 28°C. For the infection assays, bacteria were cultured in Luria-Bertani (LB) medium containing 10 mM $MgCl_2$ at 28°C.

Molecular cloning

All constructs were generated using standard molecular biology procedures. All new vectors are summarized in Table 3. All binary plasmids were transformed into *Agrobacterium tumefaciens* GV3101 (pMP90) by freeze-thawing and selected for kanamycin resistance.

The full-length *BGAL1* open reading frame and its catalytic mutant (*BGAL1*^{E183A,E254A}) were commercially synthesized without the sequence encoding the signal peptide (SeqA, Biomatik, Cambridge, Ontario, Canada). The synthetic sequence (SeqA) contained flanking *Xho*I/*Sal*I

and *Bam*HI restriction sites and a sequence encoding an *N*-terminal StrepII tag. The synthetic sequences were received in pBluescript (pBS) cloning vectors pBK23 and pBK25 for WT and mutant BGAL1, respectively. The open reading frame was cloned into the pRH509 binary vector (*44*) using *Sal*I and *Bam*H1 restriction sites, in between the *35S* promoter with a sequence encoding the PR1a signal peptide, and the *PI-II* terminator sites, resulting in binary vectors pBK26 (WT BGAL1) and pBK27 (mutant BGAL1), respectively.

The 281-bp fragment of *BGAL1* (SeqB) used for VIGS was commercially synthesized (Biomatik, Cambridge, Ontario, Canada) and was received in pBS vector pBK30. The fragment was cloned into binary TRV2 vector (*45*) using *Eco*R1 and *Bam*H1 restriction sites, resulting in binary vector pBK46.

The two CRISPR/Cas9 sgRNAs targeting BGAL were designed to minimize off-targets by using "CCTop - CRISPR/Cas9 target online predictor" (*46*), and their on-target activity was predicted according to Doench *et al.* (*47*). A CRISPR-Cas9 cloning vector (pL1V2-Kan-Cas9) was constructed by combining pAGM4723 [Addgene 48015 (*48*)] with pICH47742 [Addgene 49771 (*49*)], pICSL11017 (Addgene 51144) and pICH47761 [Addgene 48003 (*48*)] in a Golden Gate reaction with *Bpi*I, resulting in pJK236. Specific PCR products were generated by amplifying from the template for sgRNAs pICH86966 [Addgene 46966 (*12*)] using forward primers 5′-ttggtctcaattggccgtcaatgaccaacgccgttttagagctagaaatagcaag-3′ (for *sgRNA_147*/bgal1-1) or 5′-ttggtctcaattggccgaagttcgttcccccggttttagagctagaaatagcaag-3′ (for *sgRNA_106/bgal1-2*) and reverse primer 5′-ttggtctcaagcgtaatgccaactttgtac-3′. The two PCR products were combined with pJK236 and the AtU6 promoter [pICSL01009, Addgene 46968 (*12*)] in a Golden Gate reaction with *Bsa*I to generate pBK13 (*for sgRNA_106/bgal1-2*) and pBK14 (*sgRNA_147/bgal1-1*), respectively.

Table 1. *Arabidopsis* mutants lines used in this study. NASC, Nottingham Arabidopsis Stock Centre.

Name	Locus	Origin	Reference	Provided by
sd1-29	At1g61380	SAIL_857_E06	(*13*)	NASC
cerk1-2	At3g21630	GABI_096F09	(*71*)	A. Gust, Thübingen
lym1-1/lym3-1	At1g21880/At1g77630	GABI_419G07 SALK_111212	(*15*)	A. Gust, Thübingen
bak1-4	At4g33430	SALK_116202C	(*72*)	NASC
sobir1-12	At2g31880	SALK_050715	(*73*)	M. Joosten, Wageningen
fls2c	At5g46330	SAIL_691C4	(*74*)	C. Zipfel, Norwich

Table 2. *P. syringae* strains used in this study. Rif, rifampicin; –, not applicable.

Strain	Selection	Reference
Pseudomonas syringae pv. *tomato* DC3000 Δ*hQ*	Rif	(*8*)
Pseudomonas syringae pv. *tomato* DC3000 Δ*hQ*Δ*fliC*	Rif	(*18*)
Pseudomonas syringae pv. *tomato* DC3000 Δ*hrpR*	Rif	(*75*)
Pseudomonas syringae pv. *tomato* DC3000 Δ*hrpS*	Rif	(*75*)
Pseudomonas syringae pv. *tomato* DC3000 Δ*hrpL*	Rif	(*75*)
Pseudomonas syringae pv. *tomato* DC3000 Δ*hrpA*	Rif	(*76*)
Pseudomonas syringae pv. *tomato* DC3000 Δ*hrcC*	Rif	(*76*)
Pseudomonas syringae pv. *tabaci* 6605	–	(*77*)
Pseudomonas syringae pv. *tabaci* 6605 Δ*fliC*	–	(*77*)
Pseudomonas syringae pv. *tabaci* 6605 Δ*fgt1*	–	(*27*)
Pseudomonas syringae pv. *tabaci* 6605 Δ*vioT*	–	(*28*)
Pseudomonas syringae pv. *tabaci* 6605 Δ*vioA*	–	(*28*)
Pseudomonas syringae pv. *tabaci* 6605 Δ*vioB*	–	(*28*)
Pseudomonas syringae pv. *tabaci* 6605 S143A	–	(*27*)
Pseudomonas syringae pv. *tabaci* 6605 S164A	–	(*27*)
Pseudomonas syringae pv. *tabaci* 6605 S176A	–	(*27*)
Pseudomonas syringae pv. *tabaci* 6605 S183A	–	(*27*)
Pseudomonas syringae pv. *tabaci* 6605 S193A	–	(*27*)
Pseudomonas syringae pv. *tabaci* 6605 S201A	–	(*27*)
Pseudomonas syringae pv. *syringae* B728a	–	(*78*)

Table 3. Binary vectors generated in this study. T-DNA, transferred DNA.

Name	Description
pBK26	Binary vector carrying *35S::BGAL1* (SeqA) and *NptII* on T-DNA
pBK27	Binary vector carrying *35S::BGAL1*^{E183A,E254A} and *NptII* on T-DNA
pBK13	Binary vector carrying *sgRNA_106*, *Cas9* and *NptII* on T-DNA, used to generate *bgal1-2*
pBK14	Binary vector carrying *sgRNA_147*, *Cas9* and *NptII* on T-DNA, used to generate *bgal1-1*
pBK46	Binary vector carrying TRV2 with 281-bp fragment (SeqB) of BGAL1 on T-DNA

SeqA (synthetic BGAL1-encoding sequence): **Bold underlined**: Codons encoding active site glutamates were mutated into *GCA* and *GCG* in the *BGAL1*^{E183A,E254A} catalytic mutant. Underlined: SeqB used for VIGS. **Bold**: Restriction sites. *Italic with asterisk above*: Two silent substitutions introduced to remove *Eco*RI sites.

5′-at**gtcgacctcgag**ctggtctcatcctcaatttgaaaagGCCAATGTGACGTATGATCACCGGGCGTTGGTCATTGACGGCCAGCGTAGAGTTCTCATCTCCGGCTCCATACATTACCCTCGTAGTACTCCTGATATGTGGCCAGACCTTATACAGAAATCTAAAGATGGAGGATTGGATGTACTAGAGACATATGTTTTCTGGAACATACATGAACCTGTTAGAAATCAGTATGATTTTGAAGGAAGGAAAGATTTGGTTAAATTTGTGAAGTTGGTGGGGAAAGCTGGCTTATATGCTCATATAAGGATCGGGCCTTATGTTTGTGCAGAATGGAACTATGGTGGGTTTCCTCTTTGGTTGCATTTCATTCCTGGAGTTGAATTTCGAACTGATAATGAACCATTCAAGGCAGAAATGAAGCGGTTTACAGCAAAAATTGTTGACATGCTCAAGCAAGAAAATCTTTATGCATCCCAAGGGGGACCGGTTATTTTGTCTCAGATAGAAAAT**GAA**TATGGCAATGGGGGATATTGAGTCTCGTTATGGTCCTCGTGCCAAACCTTATGTCAACTGGGCAGCAAAAATGGCTACATCGTTGGATACAGGAGTGCCATGGGTTATGTGCCAGCAACCAGATGCCCCTGATCCCATAATAAACACTTGCAATGGATTCTATTGTGACCAATTCAAGCAGAAC*TCCGATAAGACACCCAAGATGTGGACG**GAG**AATTGGACTGGATGGTTTCTTTCTTTTGGTGGTGCTGTCCCTTACAGACCTGTGGAAGACATTGCTTTTTCTGTGGCTCGATTTTTCCAGCGAGGTGGAACCTTTCAGAACTATTACATGTACCACGGGGGAACGAACTTCGGCCGGACCAGTGGTGGGCCATTTATTTCAACTAGCTATGACTATGATGCTCCTTTAGATGAGTATGGCCTTATAAGACAACCAAAGTGGGGCCACTTGAAAGATCTCCATAAAGCCATAAAGCTGTGCGAGGCTGCAATGGTGGCAACTGATCCAACTATCACTTCTCCAGGATCTAACATAGAGGTCAGTGTTTATAAAACTGGATCGGTGTGTGCTGCATTTCTTGCCAATGTGGGTACACAGTCTGACGCAGCCGTGACTTTCAATGGAAATTCATATCATTTGCCTCCTTGGTCCGTGAGCATCTTACCTGATTGCAAAAATGTGGCATTTAGT-

ACTGCAAAGATTAACTCGATGTCAACAATCT-CAAAGTTTGTTACTCAGTCTACGGAAGCTG-ATGGTTCTGGCGCATCCTTGTCAGGTTGGAC-TTGGGTTAATGAGCCTGTAGGTATCTCAAGTG-ATAACGCGTTCACAAAAACGGGTTTGATGG-AGCAGATAAATACTACAGCAGATAAAAGTGA-TTATCTTTGGTACTCTCTGAGTGTTAATGTA-AAAAATGACGAGCCTTTCCTTCAAGATGGAT-CTCAAACAGTACTTCATGTGGAATCACTTGGC-CATGTTCTTCATGCTTTCATTAACGGAAAGCT-ATCAGGAAGTGGGAAAGGAAACAGTGGAAAT-TCTAAAGTTACAATTGATGTTCCTGTCACCCTT-GTACCTGGAGAAAACAAAATCGACCTGTTGA-GTGTGAATGTGGGGCTTCAGAACTATGGAGC-ATTCTTTGATCTTAAGGGAGCAGGTATTACCG-GTCCTGTGCAATTGAAAGGCTTCAAAAATGGC-TCTACTATTGATCTTTCGTCAAAGCAATGGA-CATATCAGGTTGGATTGAAAGGAGAAGAACT-GGGGTTATCTGATGGAAGTTCTTCGCTTTG-GAA*C*TCACAATCTGCATTGCCTACAAACCAAC-CATTAATTTGGTATAAGGCAAGTTTTGATG-CCCCTGCTGGAGATACCCCTCTTTCACTAG-ATTTTACTGGAATGGGAAAGGGTGAAGCA-TGGGTGAATGGACAAAGCATTGGCCGATTT-TGGCCTACCAATACTGCATCAAATGGAGGTT-GTACTGACTCCTGCAATTATAGAGGATCTTA-CAATTCTAACAAATGTCTTAAAAATTGTGGAA-AACCATCCCAGCTGCTATACCACGTTCCTCGT-TCATGGCTGCAATCCACGGGAAATGTCATAG-TGTTGTTTGAGGAAATGGGTGGGAATCCAAC-AAAGCTATCTTTTGCAACAAGAGAGACAAGT-AGTATATGCTCACGAGTTTCAGAGGCGCAT-CCACTTCCTATTGACAAGTGGACGTCGGATG-ACGATGCACGAAAGAAAGTAGGGCCAACTCT-GTCTCTTGAGTGCCCTCGTCCTGATCAAGTC-ATTTCTTCAATCAAATTTGCAAGCTTTGGC-ACTCCTCTTGGTGCATGTGGAAGCTTTA-GCCATGGTCGATGCACAAGCAACAATGCTCT-TTCCCATGTAAAGAAGGCTTGCATTGGATCG-AGACACTGTAGTGTTGGAGTTTCAATAGATG-TATTTGGTGATCCATGTATAGGAGTCACAA-AAAGTTTAGCCGTAGAAGCTTCCTGTTCG-**ggatcc**-*3′*

SeqB (fragment used for silencing BGAL1): **Bold**: Restriction sites.

5′-**gaattc**CTGTTAGAAATCAGTATGATTTTGAA-GGAAGGAAAGATTTGGTTAAATTTGTGAAGT-TGGTGGGGAAAGCTGGCTTATATGCTCATATA-AGGATCGGGCCTTATGTTTGTGCAGAATGGA-ACTATGGTGGGTTTCCTCTTTGGTTGCATTTC-ATTCCTGGAGTTGAATTTCGAACTGATAATGA-ACCATTCAAGGCAGAAATGAAGCGGTTTACA-GCAAAAATTGTTGACATGCTCAAGCAAGAAA-ATCTTTATGCATCCCAAGGGGGACCGGTTAT-TTTG**ggatcc**-*3′*

sgRNA_106 (for *bgal1-2*): Underlined: Spacer sequence.

5′-GGCCGAAGTTCGTTCCCCCGGTTTTAGAGC-TAGAAATAGCAAGTTAAAATAAGGCTAGTCC-GTTATCAACTTGAAAAAGTGGCACCGAGTCG-GTGCTTTTTTT-*3′*

sgRNA_147 (for *bgal1-1*): Underlined: Spacer sequence.

5′-GGCCGTCAATGACCAACGCCGTTTTAGAG-CTAGAAATAGCAAGTTAAAATAAGGCTAGTC-CGTTATCAACTTGAAAAAGTGGCACCGAGTC-GGTGCTTTTTTT-*3′*

Plant transformation

Agrobacterium mediated transformation of *N. benthamiana* was performed as described (*50*). Briefly, 4-week-old *N. benthamiana* plants were agroinfiltrated with *A. tumefaciens* strain GV3101 pMP90 carrying binary plasmids pBK13 (carrying sgRNA_106 for *bgal1-2*) and pBK14 (carrying sgRNA_147 for *bgal1-1*). At 3 days post-infiltration, the infiltrated leaves were cut into 1-cm^2 sections and were cultured under sterile conditions on shooting media [per liter: 4.3 g MS basal salts (1×), 30 g sucrose, 1× B5 vitamins, 0.1 mg naphthalene acetic acid (NAA), 0.59 g MES, pH 5.7 using KOH, 4 g Agargel, after autoclaving add 1 mg benzylaminopurine (BAP), 300 mg ticarcillin/clavulanic acid] for 3 days, and subsequently transferred to shooting media supplemented with 150 μg/ml kanamycin and cultured for approximately 2 to 3 weeks to select for stable transformants. Shoots were excised and transferred to rooting media [per liter: 2.15 g MS basal salts (0.5×), 5 g sucrose, 0.1 mg NAA stock, pH 5.8 with KOH, 2.5 g Gelrite, after autoclaving add 300 mg ticarcillin/clavulanic acid] supplemented with 150 μg/ml kanamycin and were further cultured until roots appeared, after which plantlets were transferred to soil and grown in the growth chamber. To identify stable *N. benthamiana* transformants carrying mutant *BGAL1* alleles, the targeted segment of the *BGAL1* gene was PCR amplified using primers for *bgal1-1* (forward primer: 5′- tctgcttctaagaacagat-3′; reverse primer: 5′-gtctctagtacatccaatcc-3′) and *bgal1-2* (forward primer: 5′-accatactcatctaaaggagca-3′; reverse primer: 5′-ggctcgatttttccagcgag-3′), and the PCR fragments were sequenced by Sanger sequencing to confirm mutations. Mutant lines were screened by ABPP using the JJB70 probe to confirm BGAL1 depletion in the T2 and T3 generations.

Virus-induced gene silencing (VIGS)

Agrobacterium cultures were grown overnight and resuspended in agroinfiltration buffer (10 mM $MgCl_2$, 10 mM MES pH 5.0, and 100 μM acetosyringone) at OD_{600} = 0.5. Bacteria containing pBK46 (*TRV::BGAL1)* or *TRV2::GFP* were mixed 1:1 with bacteria containing TRV1 (*45*). After incubation for 1 hour at room temperature, the mixed cultures were infiltrated into leaves of 10-day-old *N. benthamiana* plants. The infiltrated seedlings were grown for 3 to 4 weeks in a growth chamber until use.

Agroinfiltration

For transient expression of proteins in *N. benthamiana*, overnight cultures of *Agrobacterium* carrying binary vectors were harvested by centrifugation. Cells were resuspended in induction buffer (10 mM $MgCl_2$, 10 mM MES pH5.0, and 100 μM acetosyringone) at OD_{600} = 0.5. After 1 hour at 21°C, cells were infiltrated into leaves of 4-week-old *N. benthamiana*. Leaves were harvested and processed 4 days after agroinfiltration.

Isolation of apoplastic fluids

AFs were collected as described previously (*51*). Leaves from infected or agroinfiltrated plants were submerged in ice-cold water and infiltrated by applying vacuum for 5 min. The surface of water-infiltrated leaves were dried with absorbing paper and leaves were carefully mounted in an empty 20-ml syringe, placed in a 50-ml tube. AFs were collected by centrifugation at 2000*g* at 4°C for 20 min and used immediately.

In-solution digestion of apoplastic fluids for proteome analysis

AFs (500 μl) from *N. benthamiana* were isolated from 16 leaf discs. Proteins were reduced by incubation with dithiothreitol (DTT, final concentration 5 mM) for 30 min at room temperature. Samples were then alkylated with iodoacetamide (IAA, final concentration 20 mM) for 30 min at room temperature. Then the AFs were chloroform-methanol precipitated, and the precipitated proteins were dissolved in 100 μl of 6 M urea. 500-μl water was added and protein digestion was performed by adding 400 ng trypsin/LysC mix (Promega, Madison, WI, USA). Sample was incubated at 37°C for 18 hours. The protein digestion was stopped by adding formic acid (FA, final 1% v/v), and peptides were purified using the sep-paK C18 columns (Waters, Elstree, UK).

Proteome analysis of apoplastic fluids

Sample clean-up for LC-MS

Trypsin and LysC digested samples were desalted on homemade C18 StageTips as described (*52*). On each two-disc StageTip, peptides (~15 μg) were loaded (based on the initial protein concentration). After elution from the StageTips, samples were dried using a vacuum concentrator (Eppendorf) and the peptides were taken up into 10 μl of 0.1% formic acid solution. Samples for the analysis endogenously digested peptides in the AF were generated by supplementing the AF with four volumes of MS-grade acetone, followed by incubation on ice for 1 hour and centrifugation at 18,000*g* for 15 min. Four-fifths of the supernatants were then transferred to fresh Eppendorf tubes and the acetone evaporated by vacuum centrifugation. The dried peptide samples were then dissolved in 0.1% formic acid and immediately analyzed without further clean-up.

LC-MS/MS

Experiments were performed on an Orbitrap Elite instrument [Thermo Fisher Scientific, Waltham, MA, USA (*53*)] that was coupled to an EASY-nLC 1000 liquid chromatography (LC) system (Thermo Fisher Scientific, Waltham, MA, USA). The LC was operated in the one-column mode. For full AF analysis, the analytical column was a fused silica capillary (75 μm by 25 cm) with an integrated PicoFrit emitter (New Objective) packed in-house with Reprosil-Pur 120 C18-AQ 3-μm resin (Dr. Maisch). For analysis of endogenously digested peptides from the AF, the analytical column had a length of 35 cm and the resin was Reprosil-Pur 120 C18-AQ 1.9-μm resin (Dr. Maisch). The analytical column was encased by a column oven (Sonation) and attached to a nanospray flex ion source (Thermo Fisher Scientific, Waltham, MA, USA). The column oven temperature was adjusted

to 45°C during data acquisition. The LC was equipped with two mobile phases: solvent A (0.1% formic acid, FA, in water) and solvent B (0.1% FA in acetonitrile, ACN). All solvents were of UHPLC (ultra-high-performance liquid chromatography) grade (Sigma-Aldrich, Saint Louis, MO, USA). Peptides were directly loaded onto the analytical column with a maximum flow rate that would not exceed the set pressure limit of 980 bar (usually around 0.5 to 0.8 μl/min). Peptides were subsequently separated on the analytical column by running a 70- or 140-min gradient of solvent A and solvent B [start with 7% B; gradient 7% to 35% B for 60 (or 120 min); gradient 35% to 100% B for 5 min (or 10 min) and 100% B for 5 min (or 10 min)] at a flow rate of 300 nl/min. The mass spectrometer was operated using Xcalibur software (version 2.2 SP1.48). The mass spectrometer was set in the positive ion mode. Precursor ion scanning was performed in the Orbitrap analyzer (FTMS; Fourier transform mass spectrometry) in the scan range of m/z = 350 to 1800 and at a resolution of 60,000 with the internal lock mass option turned on [lock mass was 445.120025 m/z, polysiloxane (*54*)]. Product ion spectra were recorded in a data dependent fashion in the ion trap (ITMS; ion trap mass spectrometry) in a variable scan range and at a rapid scan rate. The ionization potential (spray voltage) was set to 1.8 to 2.0 kV. Peptides were analyzed using a repeating cycle consisting of a full precursor ion scan (1.0×10^6 ions or 30 ms) followed by 10 product ion scans (1.0×10^4 ions or 50 ms) where peptides are isolated based on their intensity in the full survey scan (threshold of 500 counts) for tandem mass spectrum (MS2) generation that permits peptide sequencing and identification. CID (collision-induced dissociation) collision energy was set to 35% for the generation of MS2 spectra. During MS2 data acquisition, dynamic ion exclusion was set to 60 s with a maximum list of excluded ions consisting of 500 members and a repeat count of one. Ion injection time prediction, preview mode for the FTMS, monoisotopic precursor selection and charge state screening were enabled. Only charge states >1 were considered for fragmentation.

Peptide and protein identification using MaxQuant

RAW spectra were submitted to an Andromeda (*55*) search in MaxQuant (version 1.5.3.30). For the analysis of trypsin/LysC digested samples, we used the following settings (*56*): Label-free quantification and match-between-runs was activated (*57*). MS/MS spectra data were searched against the ACE_0319_Niben_Final.fasta [*N. benthamiana*, 42853 entries (*6*)] and Uniprot reference database UP000002515_223283.fasta (*Pseudomonas syringae* pv. *tomato* (strain ATCC BAA-871/DC3000), 5431 entries) databases. All searches included also a contaminants database (as implemented in MaxQuant, 267 sequences). The contaminants database contains known MS contaminants and was included to estimate the level of contamination. Andromeda searches allowed oxidation of methionine residues (16 Da), acetylation of protein N terminus (42 Da) as dynamic modification, and the static modification of cysteine (57 Da, alkylation with IAM). Enzyme specificity was set to "Trypsin/P" with two missed cleavages allowed. The instrument type in Andromeda searches was set to Orbitrap and the precursor mass tolerance was set to ±20 ppm (first search) and ±4.5 ppm (main search). The MS/MS match tolerance was set to ±0.5 Da. The peptide spectrum match FDR and the protein FDR were set to 0.01 (based on target-decoy approach). Minimum peptide length was seven amino acids. For protein quantification, unique and razor peptides were allowed. Modified peptides were allowed for quantification. The minimum score for modified peptides was 40.

For the analysis of endogenously digested peptides in the AF, we used the following settings: Label-free quantification and match-between-runs was activated (*57*). MS/MS spectra data were searched against the p19_vector_proteins.fasta (two entries) and ACE_0383_SOI_v02.fasta (containing the sequence of flagellin and BGAL1). As above, all searches included also a contaminants database (as implemented in MaxQuant, 267 sequences). Andromeda searches allowed oxidation of methionine residues (16 Da) and acetylation of protein N terminus (42 Da) as dynamic modification. Enzyme specificity was set to "unspecific." The instrument type in Andromeda searches was set to Orbitrap and the precursor mass tolerance was set to ±20 ppm (first search) and ±4.5 ppm (main search). The MS/MS match tolerance was set to ±0.5 Da. The peptide spectrum match FDR and the protein FDR were set to 0.01 (based on target-decoy approach). Minimum peptide length was 8 amino acids and the maximum length 25. For protein quantification, unique and razor peptides were allowed. Modified peptides were allowed for quantification. The minimum score for modified peptides was 40.

Data analysis

Initial data analysis and filtering and statistical evaluation was performed by using the PERSEUS computational platform [version 1.5.5.3 (*58*)]. For data generated from trypsin/LysC digested samples, we performed the following manipulations: Briefly, only protein groups with at least two identified unique peptides over all runs were considered for further analysis. Non–*N. benthamiana* proteins and hits to the decoy database were removed. For quantification, we combined related biological replicates into categorical groups and investigated only those proteins that were found in all samples. Comparison of protein group quantities (relative quantification) between different MS runs is based solely on the LFQ's as calculated by MaxQuant [MaxLFQ algorithm (*57*)]. For the statistics, each biological replicate was used for a pairwise comparison. The identified proteins were plotted by the mean of the sum of Log_2(LFQ intensity) of the mock and Δ*hQ* samples against the mean of ratio(mock/Δ*hQ*) of four biological replicates. For the analysis of data generated from endogenously digested AF samples, we analyzed the peptide.txt output from MaxQuant. Peptide intensities were loaded into PERSEUS grouped into categorical groups (no_bGal or bGal) based on their treatment and normalized by subtraction from median. Missing values were then imputed and the categorical groups compared by performing a Student's *t* test (FDR 0.05; S0 0.1; number of randomizations 250). The output was visualized as volcano plot (+BGAL1 versus –BGAL1), annotated in PERSEUS and edited in CorelDraw.

TE versus AF proteomics

A comparison of an in-solution–digested *N. benthamiana* apoplastic proteome (AF) versus a leaf total extract (TE) was deposited recently (*6*). Contaminants, reverse proteins, and those only identified by matching were removed, and majority protein groups found in three out of four biological replicates of either AF or TE were retained. Log_2(sum LFQ intensity AF + TE) is plotted over the distribution (sum LFQ intensity AF)/(sum LFQ intensity AF + sum LFQ intensity TE). A ratio closer to 1 indicates predominant identification in the leaf apoplastic proteome, whereas a ratio closer to 0 indicates predominant identification in the total extract proteome.

Glycosidase activity profiling

AFs (50 μl) were incubated in 50 mM MES pH 5.0 with and without 1 μM JJB70 in the dark for 1 hour at room temperature. The labeling reaction was stopped by adding gel-loading buffer [200 mM Tris-HCl (pH 6.8), 400 mM DTT, 8% SDS, 0.4% bromophenol blue, 40% glycerol] and heating at 90°C for 5 min. The labeled proteins were separated on 10% gels at 200 volts for 1 hour.

Convolution ABPP

Two different samples were prepared for convolution ABPP. For the "label-and-mix" sample, AFs isolated from *Pto*DC3000(Δ*hQ*) infected plant (1×10^6 CFU/ml, 2 dpi), and the mock control samples (from water infiltrated plant) were first labeled individually with JJB70 for 1 hour at pH 5.0. After stopping the labeling reaction by boiling in gel-loading buffer, the labeled proteomes were mixed together in equal volumes. For the "mix-and-label" sample, equal volumes of AFs isolated from the *Pto*DC3000(Δ*hQ*)-infected and the mock control samples were first mixed, preincubated for 30 min and then labeled with JJB70 for 1 hour at pH 5.0. The labeling reaction was stopped by adding gel-loading buffer and heating at 95°C.

Detection of JJB70-labeled proteins

The fluorescently labeled proteins were detected from protein gels using the Amersham Typhoon 5 Biomolecular Imager (GE Healthcare Life Sciences, Little Chalfont, UK) using Cy2 settings (488-nm excitation and 525PB20 filter). The fluorescence was quantified using ImageQuant (GE Healthcare Life Sciences, Little Chalfont, UK).

Multiplex fluorescence ABPP

JJB70, JJB383, and FP-Tamra probes were prepared as 50 μM, 100 μM, and 10 μM stock solutions, respectively, in dimethyl sulfoxide. Labeling

was performed as described previously (*10*, *59*). For fluorescence gel imaging, the AFs were incubated with 1 μM, 2 μM, and 0.2 μM probes, respectively, for 1 hour at room temperature in the dark at a 25-μl total reaction volume. The labeling reactions were stopped by adding 4× gel-loading buffer [200 mM Tris-HCl (pH 6.8), 400 mM DTT, 8% SDS, 0.4% bromophenol blue, 40% glycerol] and heating at 90°C for 5 min. The labeled proteins were separated on 10% protein gels at 200 volts for 1 hour. The fluorescently JJB70, JJB383, and FP-Tamra-labeled proteins were detected from protein gels using the Amersham Typhoon-5 Biomolecular Imager (GE Healthcare Life Sciences, Little Chalfont, UK) using Cy2 settings (488-nm excitation and 525PB20 filter), Cy5 settings (633-nm excitation and 670PB filter), or Cy3 settings (532-nm excitation and 610PB filter), respectively.

β-galactosidase activity assays

AF samples from *N. benthamiana* leaves were incubated at 25°C with 0.2 μM fluorescein di-β-D-galactopyranoside (FDG) (Marker Gene Technologies, Eugene, OR, USA) and 50 mM MES buffer pH5.0 in the total reaction volume of 100 μl. The fluorescence of fluorescein, a product of FDG hydrolysis by β-galactosidase, was measured over time using an Infinite M200 plate reader (Tecan, Mannedorf, Switzerland) with an excitation wavelength of 485 nm and emission wavelength of 535 nm.

Colorimetric assay for glycoside hydolase activities

4-Nitrophenyl conjugates of β-D-galactopyranoside, α-D-galactopyranoside, β-D-mannopyranoside, β-D-glucopyranoside, α-D-glucopyranoside, β-D-glucuronide, β-D-xylopyranoside, α-D-xylopyranoside, β-D-fucopyranoside, *N*-acetyl-β-D-glucosaminide, *N*-acetyl-α-D-glucosaminide, *N*-acetyl-β-D-galactosaminide, and *N*-acetyl-α-D-galactosaminide (Sigma-Aldrich, Saint Louis, MO, USA) were prepared as 10 mM stock solutions in water. AFs from agroinfiltrated plants were incubated with 1 mM of each 4-nitrophenyl conjugate of monosaccharide buffered with 50 mM MES at pH 5 for 10 min at 21°C. The reactions were stopped by adding 1 M Na_2CO_3, and the released 4-nitrophenol was measured by monitoring absorbance at 420 nm using an Infinite M200 plate reader (Tecan, Mannedorf, Switzerland).

Fractionation apoplastic proteomes

AFs isolated from *Pto*DC3000(Δ*hQ*) infected leaves were concentrated using Vivaspin 500 spin columns with 3000-Da MWCO filter (Sartorius Stedim Biotech, Göttingen, Germany) by centrifuging at 10,000*g*, 4°C for 60 min. The concentrate (>3 kDa) and filtrate (<3 kDa) were normalized to equal starting volumes and used for mixing and labeling assays.

Metabolite extraction

*Pto*DC3000(Δ*hQ*) was inoculated at OD_{600} = 0.5 and grown in mannitol-glutamate minimal medium supplemented with iron (*60*). The overnight grown bacterial culture was centrifuged and supernatant was collected. Chloroform-methanol precipitation was performed by adding 4 ml of extraction buffer (1:2.5:1 of chloroform-methanol-water) to 4 ml of supernatant or only the medium as control. The sample was vortexed and centrifuged. The upper hydrophilic (methanol:water) phase and the lower hydrophobic (chloroform) phase were collected and lyophilized. The lyophilized samples were dissolved in water and concentrated using ultrafiltration spin columns to remove the <3 kDa low–molecular weight compounds. The filtrate fractions were collected and treated with and without heating at 95°C for 5 min.

Bacterial growth upon spray inoculation

For spray inoculations, an overnight culture was washed and resuspended in sterile water to a density of 1×10^8 CFU/ml and sprayed onto leaf abaxial and adaxial surfaces of 3-week-old plants. Before inoculation, eight plants per genotype were incubated at 80% humidity for 1 day. Upon inoculation, plants were kept for 3 to 4 days in a growth cabinet at 21°C. Three leaf discs (1-cm diameter) were excised from infected leaves and each leaf disc (3.2-mm diameter) was soaked in 15% H_2O_2 for 1 min to sterilize leaf surfaces. Leaf discs were washed twice in sterile water and ground in sterile water for 5 min using the tissuelyser and metal beads (Biospec Products, Bartelsville, OK, USA). Serial dilutions of the homogenate were plated onto KB agar plates without selection for *Pta6605* strains or containing 50 μg/ml rifampicin for *Pto*DC3000 strains. Colonies were counted after 36 hours of incubation at 28°C. The *P* value was calculated using the two-tailed Student *t* test to compare bacterial growth between WT and *BGAL1* mutant plants.

Bacterial growth assay in vitro

Bacteria were harvested from an overnight preculture in LB medium, washed with sterile water, and inoculated in 150 μl of the specified medium with the initial OD_{600} of 0.05. Bacterial growth was then monitored with the measurement of OD_{600} over time using Infinite M200 plate reader (Tecan, Mannedorf, Switzerland) at 28°C with shaking.

Isolation of flagellin proteins

Flagellin proteins were purified following the previously described procedure (*27*).

Oxidative burst assays

The generation of ROS was measured by a luminol-based assay on leaf discs adapted from (*61*). Luminol (Sigma-Aldrich, Saint Louis, MO, USA) was dissolved in dimethyl sulfoxide at a concentration of 10 mg/ml, and kept in the dark. Horseradish peroxidase (HRP) (Thermo Fisher Scientific, Waltham, MA, USA) was dissolved in water at a concentration of 10 mg/ml. Leaf discs (6-mm diameter) were incubated overnight in water in a 96-well plate. Bacterial pellets of an overnight culture were washed with sterile water and resuspended to an OD_{600} of 0.005 and 0.05 for *Pto*DC3000 and *Pta6605* stains in 5 ml AF from leaves of *N. benthamiana* plants transiently expressing the indicated proteins. After 1 hour of incubation at 21°C, bacteria were centrifuged and resuspended in 2.5 ml of assay solution (water with 25 ng/μl luminol and 25 ng/μl HRP). For assays with purified flagellin, 10 ng/μl of flagellin were incubated in AF (ratio 1:15) from *N. benthamiana* leaves transiently expressing the indicated proteins for 1 hour and 30 min at RT on a rotor. After incubation, 25 ng/μl luminol and 25 ng/μl HRP were added to the AF. Before measurement, the water was removed from the 96-well plate, and 100 μl of assay solution was added to the leaf discs. Chemiluminescence was recorded immediately using an Infinite M200 plate reader (Tecan, Mannedorf, Switzerland) every minute for 1 hour. Standard errors were calculated at each time point and for each treatment. Experiments were repeated at least twice.

For protease inhibition experiments, AFs were first incubated with 1× Protease Inhibitor Cocktail (Sigma) for 1 hour at room temperature. An overnight culture of *Pta6605*(Δ*fgt1*) was pelleted and resuspended in sterile water. Bacteria were added to the AF mixture to a final OD_{600} of 0.5. Alternatively, flg22 peptide was added to a final concentration of 100 nM. After a 1-hour incubation at RT, luminol and HRP were added to the solution to final concentrations of 30 ng/μl and 20 ng/μl, respectively. ROS generation was then measured as described above.

Flagellin modelling

The *Pst*DC3000 FliC protein sequence was modeled on 5wk6 [cryo-EM structure of *P. aeruginosa* flagellar filaments G420A (*62*)] using SWISS MODEL (*63*) and visualized using PyMol. The best template (homo-41-mer of *P. aeruginosa* flagellin, 56.38% sequence identity) was identified with HHblits (*64*) and the model was built using ProMod3 version 1.1.0. The model quality parameters were: QMQE = 0.75 and QMEAN = −3.34.

RT-PCR

RNA was extracted by the addition of five volumes of Trizol and one volume of chloroform to ground tissue. After brief incubation on ice, samples were separated by centrifugation and the upper aqueous phase retained. RNA was pelleted by the addition of isopropanol and centrifugation at 12,000*g*. The pellet was washed in 70% ethanol, air dried, and then resuspended in RNase-free water. cDNA synthesis was performed using the Superscript II kit (Invitrogen, Carlsbad, CA, USA). The resulting cDNA was diluted 10 times and used as a template for PCR using the Mango Taq kit (Bioline, London, UK) with the primers for BGAL1 (5′atgtgacgtatgatcaccgggg-3′ and 5′-agctttccc-caccaacttca-3′) and GAPDH [5′-agctcaagggaattctc-gatg-3′ and 5′-aaccttaaccatgtcatctccc-3′ (*65*)]. cDNA was amplified with a T_m of 53°C for 38 cycles.

Phylogenetic analysis

Arabidopsis and tomato GH35-domain containing proteins (PF01301) were retrieved from GenBank

(*Arabidopsis* RefSeq proteins and NCBI *Solanum lycopersicum* annotation release 103). *N. benthamiana* GH35-domain containing proteins were extracted from the reannotated gene-models (*6*) and manually verified against the draft genome of *N. benthamiana* (*66*). Partial sequences and putative non-protein-encoding pseudogenes were cross-validated against the other available draft genomes (*67*). For putative pseudogenes, the closest BLAST hit in other *Nicotiana* species was used to visualize pseudogenization in the phylogenetic tree. Sequences were aligned with Clustal Omega (*68*), and the amino acid residues corresponding to BGAL1 (Nbv0.3scaffold63813_1713-9438) position 26-732 [lacking the signal peptide and the Gal-Lectin domain (PF02140)] were extracted and realigned using Clustal Omega. The evolutionary history was inferred by using the maximum likelihood method based on the Le_Gascuel_2008 model (*69*). The tree with the highest log likelihood (−36048.75) is shown. The percentage of trees in which the associated taxa clustered together in 1000 bootstrap repetitions is shown next to the branches. Initial tree(s) for the heuristic search were obtained automatically by applying Neighbor-Join and BioNJ algorithms to a matrix of pairwise distances estimated using a JTT model, and then selecting the topology with superior log likelihood value. A discrete Gamma distribution was used to model evolutionary rate differences among sites [five categories (+G, parameter = 1.0633)]. The rate variation model allowed for some sites to be evolutionarily invariable ([+I], 5.50% sites). The tree is drawn to scale, with branch lengths measured in the number of substitutions per site. The analysis involved 72 amino acid sequences. Evolutionary analyses were conducted in MEGA X (*70*).

Statistics

All values shown are mean values, and the error intervals shown represent standard error of the mean (SE), unless otherwise indicated. *P* values were calculated using two-tailed Student's *t* test or Tukey HSD test, as indicated. All experiments have been reproduced, and representative datasets are shown.

REFERENCES AND NOTES

1. M. Lindeberg, Genome-enabled perspectives on the composition, evolution, and expression of virulence determinants in bacterial plant pathogens. *Annu. Rev. Phytopathol.* **50**, 111–132 (2012). doi: 10.1146/annurev-phyto-081211-173022; pmid: 22559066
2. T. Boller, G. Felix, A renaissance of elicitors: Perception of microbe-associated molecular patterns and danger signals by pattern-recognition receptors. *Annu. Rev. Plant Biol.* **60**, 379–406 (2009). doi: 10.1146/annurev.arplant.57.032905.105346; pmid: 19400727
3. D. Couto, C. Zipfel, Regulation of pattern recognition receptor signalling in plants. *Nat. Rev. Immunol.* **16**, 537–552 (2016). doi: 10.1038/nri.2016.77; pmid: 27477127
4. H. Cui, T. Xiang, J. M. Zhou, Plant immunity: A lesson from pathogenic bacterial effector proteins. *Cell. Microbiol.* **11**, 1453–1461 (2009). doi: 10.1111/j.1462-5822.2009.01359.x; pmid: 19622098
5. J. Fliegmann, G. Felix, Immunity: Flagellin seen from all sides. *Nat. Plants* **2**, 16136 (2016). doi: 10.1038/nplants.2016.136; pmid: 27595659
6. J. Kourelis, F. Kaschani, F. M. Grosse-Holz, F. Homma, M. Kaiser, R. A. L. van der Hoorn, Re-annotated *Nicotiana benthamiana* gene models for enhanced proteomics and reverse genetics. bioRxiv 373506 [Preprint]. 27 July 2018. doi: 10.1101/373506
7. F. Grosse-Holz *et al*., The transcriptome, extracellular proteome and active secretome of agroinfiltrated *Nicotiana benthamiana* uncover a large, diverse protease repertoire. *Plant Biotechnol. J.* **16**, 1068–1084 (2018). doi: 10.1111/pbi.12852; pmid: 29055088
8. C. F. Wei *et al*., A *Pseudomonas syringae* pv. tomato DC3000 mutant lacking the type III effector HopQ1-1 is able to cause disease in the model plant *Nicotiana benthamiana*. *Plant J.* **51**, 32–46 (2007). doi: 10.1111/j.1365-313X.2007.03126.x; pmid: 17559511
9. W. W. Kallemeijn *et al*., Novel activity-based probes for broad-spectrum profiling of retaining β-exoglucosidases in situ and in vivo. *Angew. Chem. Int. Ed.* **51**, 12529–12533 (2012). doi: 10.1002/anie.201207771; pmid: 23139194
10. B. Chandrasekar *et al*., Broad-range glycosidase activity profiling. *Mol. Cell. Proteomics* **13**, 2787–2800 (2014). doi: 10.1074/mcp.O114.041616; pmid: 25056938
11. B. Chandrasekar, T. N. Hong, R. A. L. van der Hoorn, Inhibitor discovery by convolution ABPP. *Methods Mol. Biol.* **1491**, 47–56 (2017). doi: 10.1007/978-1-4939-6439-0_4; pmid: 27778280
12. V. Nekrasov, B. Staskawicz, D. Weigel, J. D. Jones, S. Kamoun, Targeted mutagenesis in the model plant *Nicotiana benthamiana* using Cas9 RNA-guided endonuclease. *Nat. Biotechnol.* **31**, 691–693 (2013). doi: 10.1038/nbt.2655; pmid: 23929340
13. S. Ranf *et al*., A lectin S-domain receptor kinase mediates lipopolysaccharide sensing in Arabidopsis thaliana. *Nat. Immunol.* **16**, 426–433 (2015). doi: 10.1038/ni.3124; pmid: 25729922
14. A. Miya *et al*., CERK1, a LysM receptor kinase, is essential for chitin elicitor signaling in Arabidopsis. *Proc. Natl. Acad. Sci. U.S.A.* **104**, 19613–19618 (2007). doi: 10.1073/pnas.0705147104; pmid: 18042724
15. R. Willmann *et al*., Arabidopsis lysin-motif proteins LYM1 LYM3 CERK1 mediate bacterial peptidoglycan sensing and immunity to bacterial infection. *Proc. Natl. Acad. Sci. U.S.A.* **108**, 19824–19829 (2011). doi: 10.1073/pnas.1112862108; pmid: 22106285
16. L. Gómez-Gómez, T. Boller, FLS2: An LRR receptor-like kinase involved in the perception of the bacterial elicitor flagellin in Arabidopsis. *Mol. Cell* **5**, 1003–1011 (2000). doi: 10.1016/S1097-2765(00)80265-8; pmid: 10911994
17. C. Segonzac *et al*., Hierarchy and roles of pathogen-associated molecular pattern-induced responses in *Nicotiana benthamiana*. *Plant Physiol.* **156**, 687–699 (2011). doi: 10.1104/pp.110.171249; pmid: 21478366
18. B. H. Kvitko *et al*., Deletions in the repertoire of *Pseudomonas syringae* pv. *tomato* DC3000 type III secretion effector genes reveal functional overlap among effectors. *PLOS Pathog.* **5**, e1000388 (2009). doi: 10.1371/journal.ppat.1000388; pmid: 19381254
19. G. Felix, J. D. Duran, S. Volko, T. Boller, Plants have a sensitive perception system for the most conserved domain of bacterial flagellin. *Plant J.* **18**, 265–276 (1999). doi: 10.1046/j.1365-313X.1999.00265.x; pmid: 10377992
20. S. Robatzek *et al*., Molecular identification and characterization of the tomato flagellin receptor LeFLS2, an orthologue of Arabidopsis FLS2 exhibiting characteristically different perception specificities. *Plant Mol. Biol.* **64**, 539–547 (2007). doi: 10.1007/s11103-007-9173-8; pmid: 17530419
21. D. R. Hann, J. P. Rathjen, Early events in the pathogenicity of Pseudomonas syringae on Nicotiana benthamiana. *Plant J.* **49**, 607–618 (2007). doi: 10.1111/j.1365-313X.2006.02981.x; pmid: 17217460
22. R. Takai, A. Isogai, S. Takayama, F. S. Che, Analysis of flagellin perception mediated by flg22 receptor OsFLS2 in rice. *Mol. Plant Microbe Interact.* **21**, 1635–1642 (2008). doi: 10.1094/MPMI-21-12-1635; pmid: 18986259
23. Y. Rossez, E. B. Wolfson, A. Holmes, D. L. Gally, N. J. Holden, Bacterial flagella: Twist and stick, or dodge across the kingdoms. *PLOS Pathog.* **11**, e1004483 (2015). doi: 10.1371/journal.ppat.1004483; pmid: 25590430
24. K. Chiku *et al*., Comparative analysis of flagellin glycans among pathovars of phytopathogenic Pseudomonas syringae. *Carbohydr. Res.* **375**, 100–104 (2013). doi: 10.1016/j.carres.2013.04.018; pmid: 23694710
25. M. Yamamoto *et al*., Identification of genes involved in the glycosylation of modified viosamine of flagellins in Pseudomonas syringae by Mass Spectrometry. *Genes* **2**, 788–803 (2011). doi: 10.3390/genes2040788; pmid: 24710292
26. S. Lee, D. S. Yang, S. R. Uppalapati, L. W. Sumner, K. S. Mysore, Suppression of plant defense responses by extracellular metabolites from *Pseudomonas syringae* pv. *tabaci* in *Nicotiana benthamiana*. *BMC Plant Biol.* **13**, 65 (2013). doi: 10.1186/1471-2229-13-65; pmid: 23597256
27. F. Taguchi *et al*., Identification of glycosylation genes and glycosylated amino acids of flagellin in *Pseudomonas syringae* pv. *tabaci*. *Cell. Microbiol.* **8**, 923–938 (2006). doi: 10.1111/j.1462-5822.2005.00674.x; pmid: 16681835
28. L. C. Nguyen *et al*., Genetic analysis of genes involved in synthesis of modified 4-amino-4,6-dideoxyglucose in flagellin of *Pseudomonas syringae* pv. *tabaci*. *Mol. Genet. Genomics* **282**, 595–605 (2009). doi: 10.1007/s00438-009-0489-8; pmid: 19787374
29. B. A. Vinatzer *et al*., The type III effector repertoire of *Pseudomonas syringae* pv. *syringae* B728a and its role in survival and disease on host and non-host plants. *Mol. Microbiol.* **62**, 26–44 (2006). doi: 10.1111/j.1365-2958.2006.05350.x; pmid: 16942603
30. S. R. Hind *et al*., Tomato receptor FLAGELLIN-SENSING 3 binds flgII-28 and activates the plant immune system. *Nat. Plants* **2**, 16128 (2016). doi: 10.1038/nplants.2016.128; pmid: 27548463
31. Y. Katsuragi *et al*., CD2-1, the C-terminal region of flagellin, modulates the induction of immune repsonses in rice. *Mol. Plant Microbe Interact.* **28**, 648–658 (2015). doi: 10.1094/MPMI-11-14-0372-R; pmid: 25625819
32. F. Brunner *et al*., Pep-13, a plant defense-inducing pathogen-associated pattern from Phytophthora transglutaminases. *EMBO J.* **21**, 6681–6688 (2002). doi: 10.1093/emboj/cdf667; pmid: 12485989
33. S. Oome *et al*., Nep1-like proteins from three kingdoms of life act as a microbe-associated molecular pattern in Arabidopsis. *Proc. Natl. Acad. Sci. U.S.A.* **111**, 16955–16960 (2014). doi: 10.1073/pnas.1410031111; pmid: 25368167
34. C. Ottmann *et al*., A common toxin fold mediates microbial attack and plant defense. *Proc. Natl. Acad. Sci. U.S.A.* **106**, 10359–10364 (2009). doi: 10.1073/pnas.0902362106; pmid: 19520828
35. K. Reiss *et al*., Structural and phylogenetic analyses of the GP42 transglutaminase from *Phytophthora sojae* reveal an evolutionary relationship between oomycetes and marine Vibrio bacteria. *J. Biol. Chem.* **286**, 42585–42593 (2011). doi: 10.1074/jbc.M111.290544; pmid: 21994936
36. H. Böhm *et al*., A conserved peptide pattern from a widespread microbial virulence factor triggers pattern-induced immunity in Arabidopsis. *PLOS Pathog.* **10**, e1004491 (2014). doi: 10.1371/journal.ppat.1004491; pmid: 25375108
37. H. Hirai *et al*., Glycan moiety of flagellin in *Acidovorax avenae* K1 prevents the recognition by rice that causes the induction of immune responses. *Plant Signal. Behav.* **9**, e972782 (2014). doi: 10.4161/psb.29933; pmid: 25482815
38. F. Taguchi *et al*., Post-translational modification of flagellin determines the specificity of HR induction. *Plant Cell Physiol.* **44**, 342–349 (2003). doi: 10.1093/pcp/pcg042; pmid: 12668781
39. K. Takeuchi *et al*., Flagellin glycans from two pathovars of *Pseudomonas syringae* contain rhamnose in D and L configurations in different ratios and modified 4-amino-4,6-dideoxyglucose. *J. Bacteriol.* **189**, 6945–6956 (2007). doi: 10.1128/JB.00500-07; pmid: 17644592
40. S. K. Arora, A. N. Neely, B. Blair, S. Lory, R. Ramphal, Role of motility and flagellin glycosylation in the pathogenesis of *Pseudomonas aeruginosa* burn wound infections. *Infect. Immun.* **73**, 4395–4398 (2005). doi: 10.1128/IAI.73.7.4395-4398.2005; pmid: 15972536
41. A. Hanuszkiewicz *et al*., Identification of the flagellin glycosylation system in *Burkholderia cenocepacia* and the contribution of glycosylated flagellin to evasion of human innate immune responses. *J. Biol. Chem.* **289**, 19231–19244 (2014). doi: 10.1074/jbc.M114.562603; pmid: 24841205
42. C. Schäffer, P. Messner, Emerging facets of prokaryotic glycosylation. *FEMS Microbiol. Rev.* **41**, 49–91 (2017). doi: 10.1093/femsre/fuw036; pmid: 27566466
43. A. E. Scott *et al*., Flagellar glycosylation in *Burkholderia pseudomallei* and *Burkholderia thailandensis*. *J. Bacteriol.* **193**, 3577–3587 (2011). doi: 10.1128/JB.01385-10; pmid: 21602339
44. R. A. L. Van Der Hoorn, S. Rivas, B. B. Wulff, J. D. Jones, M. H. Joosten, Rapid migration in gel filtration of the Cf-4 and Cf-9 resistance proteins is an intrinsic property of Cf proteins and not because of their association with high-molecular-

weight proteins. *Plant J.* **35**, 305–315 (2003). doi: 10.1046/j.1365-313X.2003.01803.x; pmid: 12887582
45. Y. Liu, M. Schiff, R. Marathe, S. P. Dinesh-Kumar, Tobacco Rar1, EDS1 and *NPR1/NIM1* like genes are required for *N*-mediated resistance to tobacco mosaic virus. *Plant J.* **30**, 415–429 (2002). doi: 10.1046/j.1365-313X.2002.01297.x; pmid: 12028572
46. M. Stemmer, T. Thumberger, M. Del Sol Keyer, J. Wittbrodt, J. L. Mateo, CCTop: An intuitive, flexible and reliable CRISPR/Cas9 target prediction tool. *PLOS ONE* **10**, e0124633 (2015). doi: 10.1371/journal.pone.0124633; pmid: 25909470
47. J. G. Doench *et al*., Optimized sgRNA design to maximize activity and minimize off-target effects of CRISPR-Cas9. *Nat. Biotechnol.* **34**, 184–191 (2016). doi: 10.1038/nbt.3437; pmid: 26780180
48. E. Weber, C. Engler, R. Gruetzner, S. Werner, S. Marillonnet, A modular cloning system for standardized assembly of multigene constructs. *PLOS ONE* **6**, e16765 (2011). doi: 10.1371/journal.pone.0016765; pmid: 21364738
49. K. Belhaj, A. Chaparro-Garcia, S. Kamoun, V. Nekrasov, Plant genome editing made easy: Targeted mutagenesis in model and crop plants using the CRISPR/Cas system. *Plant Methods* **9**, 39 (2013). doi: 10.1186/1746-4811-9-39; pmid: 24112467
50. I. A. Sparkes, J. Runions, A. Kearns, C. Hawes, Rapid, transient expression of fluorescent fusion proteins in tobacco plants and generation of stably transformed plants. *Nat. Protoc.* **1**, 2019–2025 (2006). doi: 10.1038/nprot.2006.286; pmid: 17487191
51. F. Grosse-Holz *et al*., Three unrelated protease inhibitors enhance accumulation of pharmaceutical recombinant proteins in *Nicotiana benthamiana*. *Plant Biotechnol. J.* **16**, 1797–1810 (2018). doi: 10.1111/pbi.12916; pmid: 29509983
52. J. Rappsilber, M. Mann, Y. Ishihama, Protocol for micro-purification, enrichment, pre-fractionation and storage of peptides for proteomics using StageTips. *Nat. Protoc.* **2**, 1896–1906 (2007). doi: 10.1038/nprot.2007.261; pmid: 17703201
53. A. Michalski *et al*., Ultra high resolution linear ion trap Orbitrap mass spectrometer (Orbitrap Elite) facilitates top down LC MS/MS and versatile peptide fragmentation modes. *Mol. Cell. Proteomics* **11**, 013698 (2012). doi: 10.1074/mcp.O111.013698; pmid: 22159718
54. J. V. Olsen *et al*., Parts per million mass accuracy on an Orbitrap mass spectrometer via lock mass injection into a C-trap. *Mol. Cell. Proteomics* **4**, 2010–2021 (2005). doi: 10.1074/mcp.T500030-MCP200; pmid: 16249172
55. J. Cox *et al*., Andromeda: A peptide search engine integrated into the MaxQuant environment. *J. Proteome Res.* **10**, 1794–1805 (2011). doi: 10.1021/pr101065j; pmid: 21254760
56. J. Cox, M. Mann, MaxQuant enables high peptide identification rates, individualized p.p.b.-range mass accuracies and proteome-wide protein quantification. *Nat. Biotechnol.* **26**, 1367–1372 (2008). doi: 10.1038/nbt.1511; pmid: 19029910
57. J. Cox *et al*., Accurate proteome-wide label-free quantification by delayed normalization and maximal peptide ratio extraction, termed MaxLFQ. *Mol. Cell. Proteomics* **13**, 2513–2526 (2014). doi: 10.1074/mcp.M113.031591; pmid: 24942700
58. S. Tyanova *et al*., The Perseus computational platform for comprehensive analysis of (prote)omics data. *Nat. Methods* **13**, 731–740 (2016). doi: 10.1038/nmeth.3901; pmid: 27348712
59. A. M. Husaini *et al*., Multiplex fluorescent, activity-based protein profiling identifies active α-glycosidases and other hydrolases in plants. *Plant Physiol.* **177**, 24–37 (2018). pmid: 29555787
60. P. A. Bronstein *et al*., Global transcriptional responses of Pseudomonas syringae DC3000 to changes in iron bioavailability in vitro. *BMC Microbiol.* **8**, 209 (2008). doi: 10.1186/1471-2180-8-209; pmid: 19055731
61. J. M. Smith, A. Heese, Rapid bioassay to measure early reactive oxygen species production in Arabidopsis leave tissue in response to living *Pseudomonas syringae*. *Plant Methods* **10**, 6 (2014). doi: 10.1186/1746-4811-10-6; pmid: 24571722
62. F. Wang *et al*., A structural model of flagellar filament switching across multiple bacterial species. *Nat. Commun.* **8**, 960 (2017). doi: 10.1038/s41467-017-01075-5; pmid: 29038601
63. A. Waterhouse *et al*., SWISS-MODEL: Homology modelling of protein structures and complexes. *Nucleic Acids Res.* **46**, W296–W303 (2018). doi: 10.1093/nar/gky427; pmid: 29788355
64. M. Remmert, A. Biegert, A. Hauser, J. Söding, HHblits: Lightning-fast iterative protein sequence searching by HMM-HMM alignment. *Nat. Methods* **9**, 173–175 (2011). doi: 10.1038/nmeth.1818; pmid: 22198341
65. D. Liu *et al*., Validation of reference genes for gene expression studies in virus-infected *Nicotiana benthamiana* using quantitative real-time PCR. *PLOS ONE* **7**, e46451 (2012). doi: 10.1371/journal.pone.0046451; pmid: 23029521
66. A. Bombarely *et al*., A draft genome sequence of *Nicotiana benthamiana* to enhance molecular plant-microbe biology research. *Mol. Plant Microbe Interact.* **25**, 1523–1530 (2012). doi: 10.1094/MPMI-06-12-0148-TA; pmid: 22876960
67. F. Naim *et al*., Advanced engineering of lipid metabolism in *Nicotiana benthamiana* using a draft genome and the V2 viral silencing-suppressor protein. *PLOS ONE* **7**, e52717 (2012). doi: 10.1371/journal.pone.0052717; pmid: 23300750
68. F. Sievers *et al*., Fast, scalable generation of high-quality protein multiple sequence alignments using Clustal Omega. *Mol. Syst. Biol.* **7**, 539 (2011). doi: 10.1038/msb.2011.75; pmid: 21988835
69. S. Q. Le, O. Gascuel, An improved general amino acid replacement matrix. *Mol. Biol. Evol.* **25**, 1307–1320 (2008). doi: 10.1093/molbev/msn067; pmid: 18367465
70. S. Kumar, G. Stecher, M. Li, C. Knyaz, K. Tamura, MEGA X: Molecular evolutionary genetics analysis across computing platforms. *Mol. Biol. Evol.* **35**, 1547–1549 (2018). doi: 10.1093/molbev/msy096; pmid: 29722887
71. S. Gimenez-Ibanez *et al*., AvrPtoB targets the LysM receptor kinase CERK1 to promote bacterial virulence on plants. *Curr. Biol.* **19**, 423–429 (2009). doi: 10.1016/j.cub.2009.01.054; pmid: 19249211
72. A. Heese *et al*., The receptor-like kinase SERK3/BAK1 is a central regulator of innate immunity in plants. *Proc. Natl. Acad. Sci. U.S.A.* **104**, 12217–12222 (2007). doi: 10.1073/pnas.0705306104; pmid: 17626179
73. M. Gao *et al*., Regulation of cell death and innate immunity by two receptor-like kinases in Arabidopsis. *Cell Host Microbe* **6**, 34–44 (2009). doi: 10.1016/j.chom.2009.05.019; pmid: 19616764
74. C. Zipfel *et al*., Bacterial disease resistance in Arabidopsis through flagellin perception. *Nature* **428**, 764–767 (2004). doi: 10.1038/nature02485; pmid: 15085136
75. C. Waite, J. Schumacher, M. Jovanovic, M. Bennett, M. Buck, Negative autogenous control of the master type III secretion system regulator hrpL in *Pseudomonas syringae*. *mBio* **8**, e02273-16 (2017). doi: 10.1128/mBio.02273-16; pmid: 28119474
76. W. Wei *et al*., The gene coding for the Hrp pilus structural protein is required for type III secretion of Hrp and Avr proteins in *Pseudomonas syringae* pv. *tomato*. *Proc. Natl. Acad. Sci. U.S.A.* **97**, 2247–2252 (2000). doi: 10.1073/pnas.040570097; pmid: 10681465
77. R. Shimizu *et al*., The DeltafliD mutant of *Pseudomonas syringae* pv. *tabaci*, which secretes flagellin monomers, induces a strong hypersensitive reaction (HR) in non-host tomato cells. *Mol. Genet. Genomics* **269**, 21–30 (2003). pmid: 12715150
78. H. Feil *et al*., Comparison of the complete genome sequences of *Pseudomonas syringae* pv. *syringae* B728a and pv. *tomato* DC3000. *Proc. Natl. Acad. Sci. U.S.A.* **102**, 11064–11069 (2005). doi: 10.1073/pnas.0504930102; pmid: 16043691

ACKNOWLEDGMENTS

We thank M. Joosten and A. Gust for providing seeds of *Arabidopsis* mutants; H. Overkleeft for providing glycosidase probes; I. Somssich for providing flg22; C. Zipfel for helpful strategic suggestions and providing *fls2c* seeds; A. Collmer for providing *Pto*DC3000 mutants; U. Pyzio for plant care; J. Baker for photography; J. Jones, S. Kamoun, and S. Marillonnet for providing plasmids via AddGene; and R. Tóth and D. Sueldo for critically reading the manuscript. **Funding:** This work was supported by ERC Consolidator grant 616449 "GreenProteases" (to P.B., K.M., R.A.L.v.d.H.), BBSRC grant BB/R017913/1 (to P.B., R.A.L.v.d.H.), a Royal Thai Government Scholarship (to N.S.), the Clarendon Foundation (to J.K.), and the Oxford Interdisciplinary Bioscience DTP (BB/M011224/1 to N.S., E.L.T., G.M.P.). **Author contributions:** P.B., B.C., N.S., G.M.P., and R.A.L.v.d.H. conceived of the project; P.B., B.C., N.S., E.L.T., and K.M. performed experiments; J.K. performed bioinformatic analysis; F.K. and M.K. performed proteomic analysis; Y.I. provided materials; and R.A.L.v.d.H. wrote the manuscript with input from all authors. **Competing interests:** The authors declare no competing interests. **Data and materials availability:** All data are available in the manuscript, supplementary materials, and cited references. The proteomics data have been deposited to the ProteomeXchange Consortium via the PRIDE partner repository (www.ebi.ac.uk/pride/archive/) with dataset identifiers PXD010461 and PXD011823.

SUPPLEMENTARY MATERIALS

www.sciencemag.org/content/364/6436/eaav0748/suppl/DC1
Figs. S1 to S18
Reference (*79*)

13 August 2018; accepted 12 February 2019
10.1126/science.aav0748

Glycosidase and glycan polymorphism control hydrolytic release of immunogenic flagellin peptides

Pierre Buscaill, Balakumaran Chandrasekar, Nattapong Sanguankiattichai, Jiorgos Kourelis, Farnusch Kaschani, Emma L. Thomas, Kyoko Morimoto, Markus Kaiser, Gail M. Preston, Yuki Ichinose, and Renier A. L. van der Hoorn

Science **364** (6436), eaav0748. DOI: 10.1126/science.aav0748

Glycosylation goes back and forth

Plants produce receptors that recognize fragments of microbial flagellin, thus monitoring for infection by bacteria. Buscaill *et al.* studied how a flagellin fragment is made accessible for recognition by host glycosidases, which degrade the glycosylations shielding the peptide that triggers the immune response. The pathogen, in turn, evades detection by altering flagellin glycosylation and inhibiting the host glycosidase. This aspect of plant defense against infection plays out in the apoplast, the extracellular space within plant tissues.

Science, this issue p. eaav0748